JMEPEG (2006) 15:355-364
DOI: 10.1361/105994906X108693

1059-9495/$19.00

Study of the Surface Nanocrystallization Induced by the Esonix Ultrasonic Impact Treatment on the Near-Surface of 2024-T351 Aluminum Alloy

X. An, C.A. Rodopoulos, E.S. Statnikov, V.N. Vitazev, and O.V. Korolkov

(Submitted June 2, 2005; in revised form September 8, 2005)

A nanocrystalline surface layer of Al alloy induced by the Esonix Ultrasonic Impact Treatment process was studied by advanced electron microscopes. The results revealed that the process can effectively refine the surface coarse grains into equiaxed nanocrystalline grains (grain size: 8.0-10.0 nm) and elongated microbands (15-20 nm wide). The surface affected zone was measured to be approximately 10 μm. The microstructural features include nanograins, microbands, high-density dislocation, and twining structure.

Keywords dislocation cell formation, enhancement of fatigue resistance, nanocrystallization

1. Introduction

The physical properties of a metal are strongly influenced by its grain size. On the basis of experimental results obtained in microcrystalline (mc) metals with grain size typically above 1 μm, it is widely recognized that an increase in grain size generally results in a reduction in the fatigue endurance limit. Recent research has indicated that grain refinement to an ultrafine crystalline (ufc) state (grain size typical in the 100 nm to 1 μm region) and nanocrystalline state (nc; grain size typically less than 100 nm) can have a substantial effect on the total life under stress-controlled fatigue and on fatigue crack growth (Ref 1).

Various deformation technologies have been introduced to produce fine grain structuring and thus achieving superior material properties without changing the chemical composition, ranging from conventional thermomechanical processing (Ref 2, 3) to severe plastic deformation (SPD) technologies (Ref 4-10).

The conventional thermomechanical processes include discontinuous recrystallization and continuous recrystallization processes. Using thermomechanical processes, the smallest grain size in aluminum is typically achieved by deformation to larger strains of alloys containing second phase particles larger than 1 μm, and subsequent annealing to stimulate recrystallization (Ref 11). The commercial Rockwell process, which produces ~10 μm grain in aluminum alloys for superplastic applications, is based on such a principle (Ref 12). However, the production of micron-grained alloys by conventional thermomechanical processing technologies is limited by the achievable strains (up to 3-4).

SPD processing is a very effective method for deforming metals using very high plastic strains with the aim of producing submicron-grained material at a relatively low cost (Ref 13). The more accessible techniques include Equal Channel Angular Extrusion (ECAE) (Ref 8, 9), accumulative roll bonding (ARB) (Ref 4), torsion under hydrostatic pressure (THP) (Ref 5), multipass-coinforge (Ref 6), and repetitive corrugation and strengthening (Ref 7). Markushev et al. (Ref 10) treated the Russian alloy 1420 (Al-Mg-Li-Zr) with several SPD methods and compared the microstructure and mechanical behavior of the materials. The results showed that complex ufc structures with grain size 0.7-1.2 μm can be obtained by the equal-channel angular pressing (ECAP) process; ufc fragment structure with grain size 0.2 μm can be achieved by the THP process; ufc with grain size 1.6 μm can be reached by the MSF process. In other works, it has been reported that with total strains of up to eight by ARB applied to Al alloys, a submicron grain size can be achieved (Ref 4). THP, which introduces strains of the order of seven, can produce grain size as fine as 0.2 μm (Ref 5). ECAE in Al alloys has brought average high angle boundary spacing <1 μm in all dimensions and fraction of high angle boundary area of 70-80% by high strain order of more than seven (Ref 14) and obtained ufc structure with a grain size of about 100 nm (Ref 15). The work of Prangnell et al. (Ref 14) indicated that submicron grain structure can be produced by SPD at temperatures of $<0.4\ T_m$, but nanocrystalline structure can only be achieved below $0.2\ T_m$ without fracture. The above works demonstrate that SPD technologies provide a wide range of grain size refinement from mc to ufc. It has been proven that ultrafine grain materials exhibited high yield strength, low strain hardening, and specific fatigue behavior that show changes in the Bauschinger energy parameter β_E with respect to the cumulative plastic strain (Ref 15). However, most of the SPD techniques are difficult to transfer into industrial scale application because of their high cost and slow production rate.

It is well known that component failure caused by fatigue, corrosion, or other forms of operational duty capable of introducing stress concentrators normally initiate on the surface.

X. An and **C.A. Rodopoulos,** Structural Materials and Integrity Research Centre, Materials and Engineering Research Institute (MERI), Sheffield Hallam University, City Campus, Howard Street, Sheffield, S1 1WB, U.K.; **E.S. Statnikov,** Applied Ultrasonics, 5871 Old Leeds Rd, Irondale, AL 35210; and **V.N. Vitazev** and **O.V. Korolkov,** Northern Scientific Technological Company, 6 Voronin Str. Severodvinsk, Arkhangelsk Region, 164500, Russian Federation. Contact e-mail: c.rodopoulos@shu.ac.uk.

Table 1 Chemical composition of 2024-T351 (wt.%)

Alloy		Si	Fe	Cu	Mn	Mg	Cr	Zn	Ti	Zr	Al
2024-T351	min	…	…	3.8	0.30	1.2	…	…	…	…	Balance
	max	0.50	0.50	4.9	0.90	1.8	0.10	0.25	0.15	…	Balance

Hence, optimization of the surface structure and properties may effectively improve the global behavior of the material. A number of SPD based processes for surface nanocrystallization, namely Esonix ultrasonic impact treatment (EUIT) (Ref 16), ultrasonic shot peeping (USSP) (Ref 17-19), and surface mechanical attrition treatment (SMAT) (Ref 20) have been commercially introduced in the recent decades and have attracted significant scientific interest because of their simplicity and low cost. The surface nanocrystallization of pure Fe and 316L stainless steel induced by USSP was reported in Ref 17 and 18 to produce a surface layer of an approximate thickness of 30 μm in which the grain size gradually changes from about 10 nm at the top surface layer to more than 100 nm at the end of the layer (Ref 17, 18). Similar, findings have been reported in the case of an aluminum alloy treated by USSP (Ref 19).

The EUIT is a technique that directly deforms the surface of materials using ultrasonic impacts (Ref 21). This technique fundamentally differs from contact methods of ultrasonic deformation treatment, the development of which dates back to the 1950s (Ref 22). The EUIT process is employing continuous ultrasonic vibrations at the ultrasonic transducer output end strengthened with hard materials (carbide-containing alloys, artificial diamonds, etc.) and being in direct and generally continuous contact with the treated surface. As a result, a relatively thin surface layer of the treated material is plastically deformed, producing modifications of the surface microstructure (fine grain size) and redistribution of residual stresses in this layer, which was wider confirmed to efficiently improve the fatigue property of the materials. However, the USSP has small penetration depth due to the rigid connection of the tool with the treated surface and requires relatively high pressing force. The above limits the areas of application of this method in industry.

The EUIT method, which is based on converting ultrasonic oscillations of the transducer into controlled impulses of ultrasonic impacts, has radically changed the situation (Ref 23-28). It provides an opportunity to achieve a specified depth regardless of the pressing force with a uniform quality of treatment of irregular surfaces of virtually any complexity, including, for example, welds. The main distinctive feature of EUIT when compared with well-known peening methods, including USSP, is that the impact parameters are controlled according to the engineering task to affect the surface, material, and its structure. The EUIT technology holds an advantage over other known techniques of improving fatigue resistance of welded structures, including surface plastic deformation methods (Ref 29).

Most of the investigations on EUIT technology have been focused on the mechanical properties of the EUIT materials, especially in terms of fatigue strength (Ref 26-29). However, a detailed description of surface microstructure of an aluminum alloy induced by the EUIT process has not been described in open publications. In the present work, the effects from the EUIT on the popular 2024-T351 aluminum alloy are investigated using scanning electron microscopy (SEM) and transmission electron microscopy (TEM). The aim of the work is to provide an understanding of the microstructure and refinement mechanisms associated with the formation of nanocrystalline (nc) microstructure of the materials.

Table 2 Basic mechanical properties of 2024-T351 according to ASTM E8m-94a

Mechanical properties	Mean	99% conf.	Standard deviation	Standard error
0.2% Yield strength, MPa	347.4	5.1	4.5	1.5
Tensile strength, MPa	484.6	2.6	2.3	0.7
Elongation, %	15.0	0.2	0.2	0.07
Fracture toughness—plane stress, MPa $m^{1/2}$, for thickness 1.6 mm	135.5	8.7	3.0	1.5
Strain energy density, MJ/m^3	70.5	0.6	0.5	0.2

Table 3 EUIT process parameters

	EUIT-ID	
EUIT process parameter	EUIT-1	EUIT-2
Carrier frequency, kHz	36	36
Pin dimension, mm	∅ 5.0× 17, R25	∅ 5.0× 17, R25
Normalized impact	64 impulses	64 impulses
Amplitude under load, μm	18	15
Pressure, kg	3	3
Impact frequency, Hz	260	220
Feed rate, mm/min	400	1000

2. Experimental Procedures

2.1 Material

The material used in this work was rolled 2024-T351 Al alloy plate provided by Airbus UK and manufactured by Alcoa. The material has a chemical composition, as shown in Table 1. The mechanical properties of the material perpendicular to the rolling direction long transverse (LT) have been obtained according to ASTM E8m-94a and are shown in Table 2.

2.2 EUIT Parameters

Two different UIT parameters have been selected for the investigation and are shown in Table 3.

The experimental setup is shown in Fig. 1.

2.3 Microstructural Characterization

The average grain size of the specimens was studied in plane view by SEM, Phillips XL 40, operating at 20 KV equipped with an energy dispersive spectrometer (EDS). The etched surface of the sample was prepared by sputtering erosion (using argon ion) of the surface using glow discharge optical emission spectrometer (GDOES), LECO GDS-750

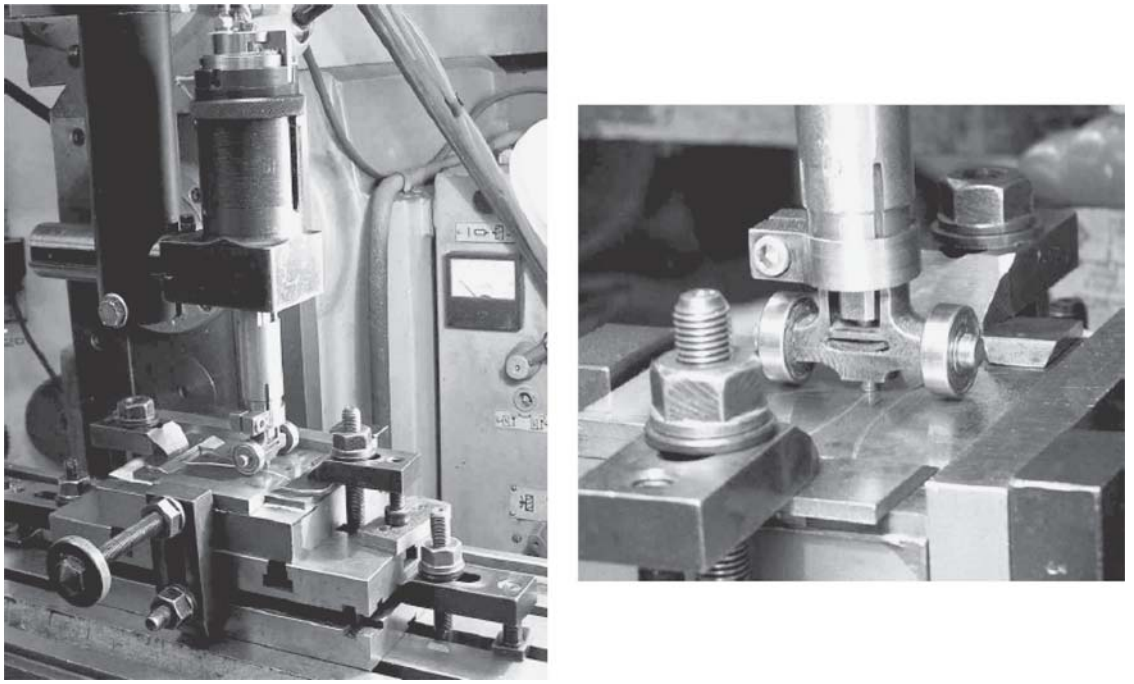

Fig. 1 EUIT Process setup in a CNC table

QDP operating at voltage 600 V, and current 25 mA. The etched depth was controlled by controlling the sputtered time ranging from 30 to 700 s. The etched depth of the specimens was then measured by a laser profilometer, which provided the depth from the top surface. The cross-sectional specimens were prepared by conventional metallographic techniques, finishing with 1 μm diamond paste. The microstructure of the specimen with the EUIT process was also examined by TEM, CM20, operating at 200 kV. Cross-sectional thin foil samples were prepared by mechanical polishing first down to 30-40 μm, and they were further thinned by the precision ion polishing system (PIPS), Gatan model 691. During ion beam thinning, an argon beam eroded the specimen surface from the back toward the surface edge. The ion beam was angled at approximately 7-6°, 5.5 kV initially, and gradually down to approximately ± 4°, 4.0 kV until a hole appeared on the specimen, which was invariable near the surface region.

3. Results

Figure 2 shows a series of compared plane view SEM images taken from different depths and provide an overview of the grain size distribution. The specimens have been sputtered by different sputtering times, which give a fresh etched surface at different depths from the top surface down to matrix of the specimen.

The results reveal that the average grain size of the material after the EUIT process has been greatly refined compared to the bare metal. The maximum visible affected zone by SEM observation was approximately 34 μm from the surface. It can be seen that at a depth of 2.6 μm from the surface, the majority of grains are significantly refined down to an average grain size of approximately 4.13 μm after the EUIT process. Herein, it is important to note that the average grain size of the bare material at this depth is approximately 16.52 μm. For larger depths, the difference in the average grain size between the bare and the UIT treated gradually decreases. At a depth of 34.5 μm, all three samples exhibited similar average grain size of approximately 36-39 μm.

Figure 2 reveals that the resulting grain size is profoundly affected by the EUIT control parameters. Slower feed rate and larger amplitude under load (EUIT1) resulted in a smaller average grain size at the subsurface (Fig. 2b) and larger average grain size at the top surface (Fig. 2a) when compared to that obtained from a faster feed rate and a lower amplitude under load (EUIT2). The feed rate predominantly controls the disposing time of the generated heat, and the amplitude is responsible for the impact strain.

The above results indicate that the average grain size of materials can be greatly reduced after EUIT treatment. However, SEM observations provide only limited resolution capability in identifying subgrain structures. Further study by TEM revealed a nanocrystalline structure surface layer induced by the EUIT1 process. Such a typical structure is shown in Fig. 3. The image was taken from the surface region of the cross sectional TEM specimen. The average grain size of the nanocrystalline structure surface layer was determined to be approximately 8-10 nm. Some grain boundaries are visible, but many grain boundaries were poorly defined at low magnification (Fig. 3a); however, high magnification imaging illustrated the formation of the equiaxed ultrafine nanograins at this top surface region (Fig. 3b).

The grain boundaries of the nanograins were well delineated, which exhibited a homogeneous contrast in the TEM bright filed image. The SAD pattern consisted of well defined rings, which indicated the generation of the finer highly disorientated grains and nanocrystalline structure. The grain boundary of a larger grain was also observed at this region (arrow), which suggested that nanocrystalline structure was produced as part of numerous subgrains. Figure 4 shows another example of the nanocrystalline structure at the surface. In

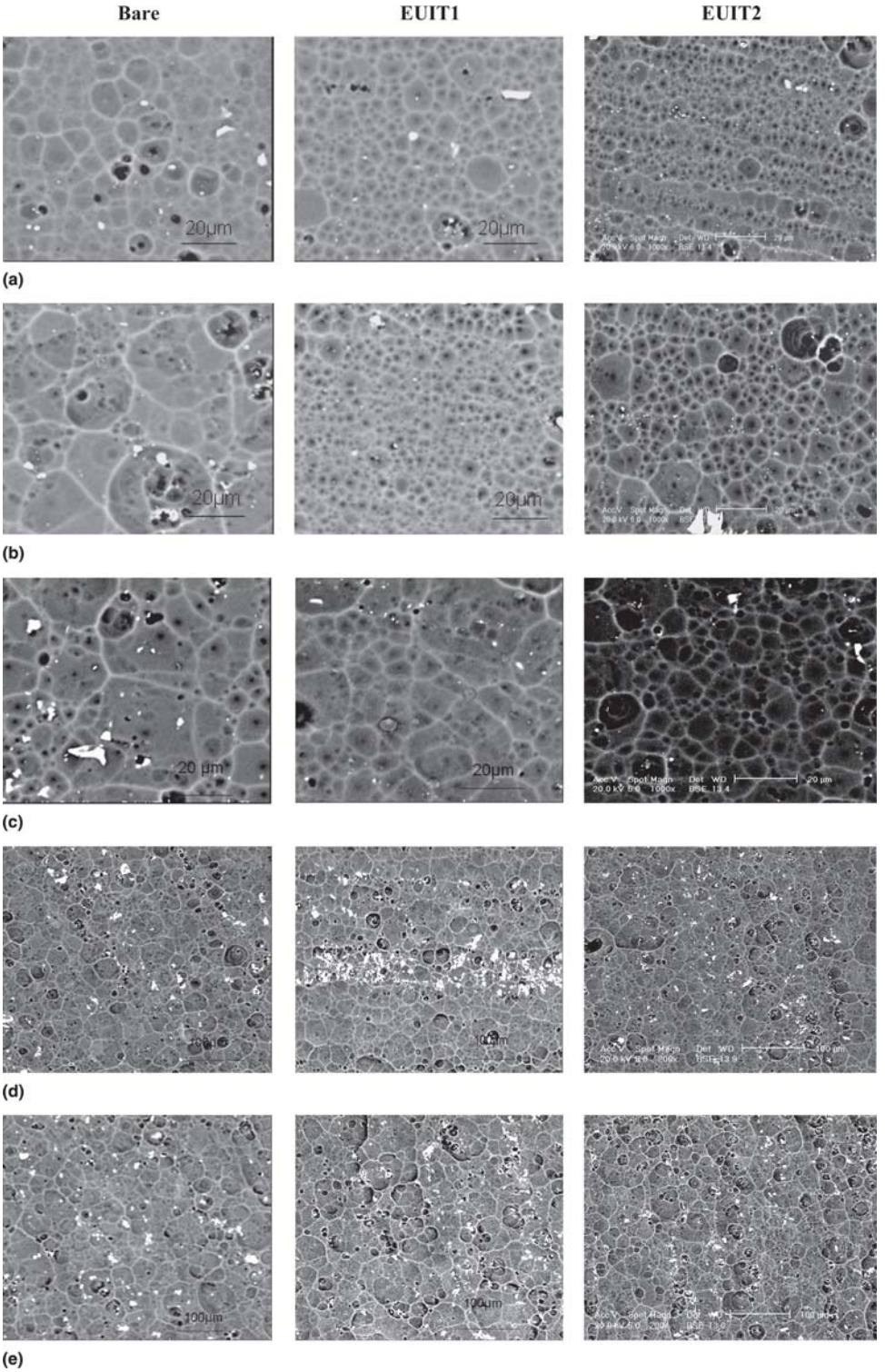

Fig. 2 Appearance of microstructure and average grain size measurements as a function of sputtering time (depth): (a) sputtering duration 30 s; depth 1.3 μm; average grain size bare 12.23 μm, EUIT1 7.75 μm, EUIT2 5.62 μm; (b) sputtering duration 80 s; depth 2.6 μm; average grain size bare 16.52 μm, EUIT1 4.13 μm, EUIT2 7.12 μm; (c) sputtering duration 120 s; depth = 4.8 μm, average grain size bare 16.96 μm, EUIT1 9.71 μm, EUIT2 6.3 μm; (d) sputtering duration 180 s; depth 7.3 μm, average grain size bare 31.01 μm, EUIT1 31.07 μm, EUIT2 23.6 μm; and (e) sputtering duration 700 s; depth 34.5 μm; average grain size bare 39.16 μm, EUIT1 36.18 μm, EUIT2 23.7 μm

this region, the grain sizes varied within a certain range, and deformation twining structure was observed within this region accompanied with ultrafine grains.

Figure 5(a) demonstrates the presence of parallel lamellar type microbands of elongated subgrains, as a result of the straining experienced during the EUIT process. The above image was taken from about 5 mm away from the region shown in Fig. 3 and shows a mixed nanocrystalline structure and

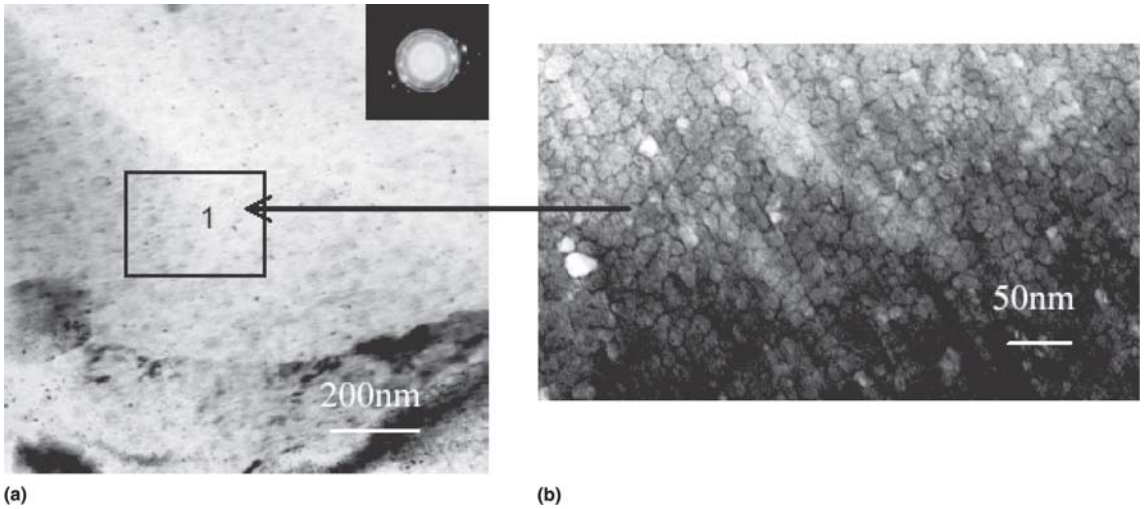

Fig. 3 TEM bright-field image showing the equiaxed nanocrystalline regimen: (a) a low magnification image, (inset) SAD demonstrates a perfect ring pattern; (b) high magnification of zone 1

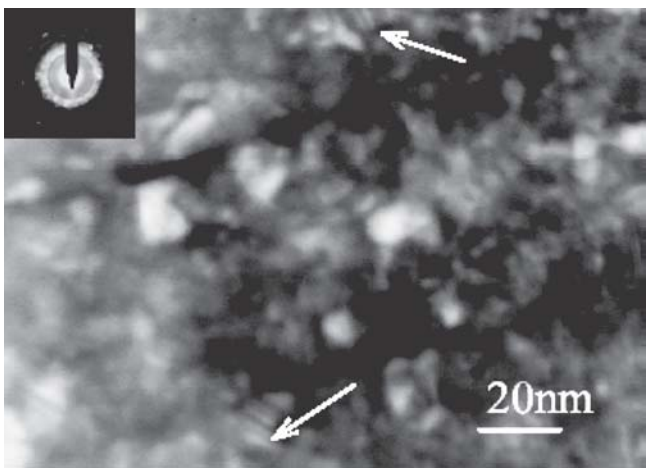

Fig. 4 TEM bright-field image of the nanocrystalline region with various grain sizes accompanied by twining structure

microbands at the outer surface region (depth at >3 μm from top surface) where the higher strain is also expected. The microbands have been measured to be about 10-15 nm wide with elongation length between 40 and 1200 nm. SAD gives an undeveloped ring pattern, which suggests the developing grain refinement process. Similar microband structure was also observed at deeper regions, >7 μm, where the strain is expected to be lower (Fig. 5b). The microbands were uniform at this region and found to be 10-15 nm wide and well elongated following the rolling direction. The SAD pattern (insert Fig. 5b) shows a developing circle with well-defined diffraction spots, indicating that microbands consisted of low angle misorientations. A twin structure was also observed within the microbands structure. TEM results indicated that this surface nanocrystalline structure was more than 10 μm deep from the surface.

Although the majority of the grains have been refined as a result of the EUIT process, the existence of coarser grains is still present (Fig. 2a and b). The above evidence indicates that ultrafine grain size may not have been formed uniformly within the alloy. SEM observations (Fig. 6) reveal that EUIT resulted into the creation of different grain size zones. In the same figure it is clear there is a connection between the creation of these zones and the distribution of precipitates in a similar manner. Considering the geometrical scale difference between the size of these zones and the diameter of the pin, explanations should be sought in terms of the role of the precipitates during the nanocrystallization process.

Examination of the precipitates using EDS identified that the precipitates were rich in Al, Cu, Fe, Mn, and Si. However, the density of the precipitates was found to exhibit a minimum at the surface and near surface of the EUIT samples (Fig. 2 and 6). Such a feature, possibly caused by dissolution-coarsening, has also been observed to take place closer to the coarser grain band region and to become more disperse within the finer grain band. In contrast, precipitate phases can be seen to be more evenly distributed within the as-rolled sample. It seems that the EUIT process caused the precipitates to migrate into certain directions and also brought the localized change in their volume fraction.

High concentration dislocation zones were also observed at the surface region of the EUIT1 sample (Fig. 7a and b). The dislocation cells (DC) were formed at the top surface region accompanied by a nanocrystalline structure (Fig. 8). The dislocation cells may well define the limits where individual subgrains can form. Figure 9 reveals the high stress distributed within the grain and disappearance at the grain boundary at a deep region of the alloy. The fine structure was observed within the grain, in which the dislocation tangle zone (DTZ) was observed. The DTZ formed near the boundary and gradually transformed into dislocation cells within the grain. Figure 10 is the image taken from the deep region of the surface layer, which clearly shows the twining boundary accompanied by a high dislocation density region within the grains.

4. Discussion

Microstructural investigation by TEM and SEM have revealed that the EUIT process produces ultrafine grain structure in the nanocrystalline regimen down to a depth from the top surface layer of about 6-10 μm. The average grain size exhibited a size increase with distance from the surface due to the

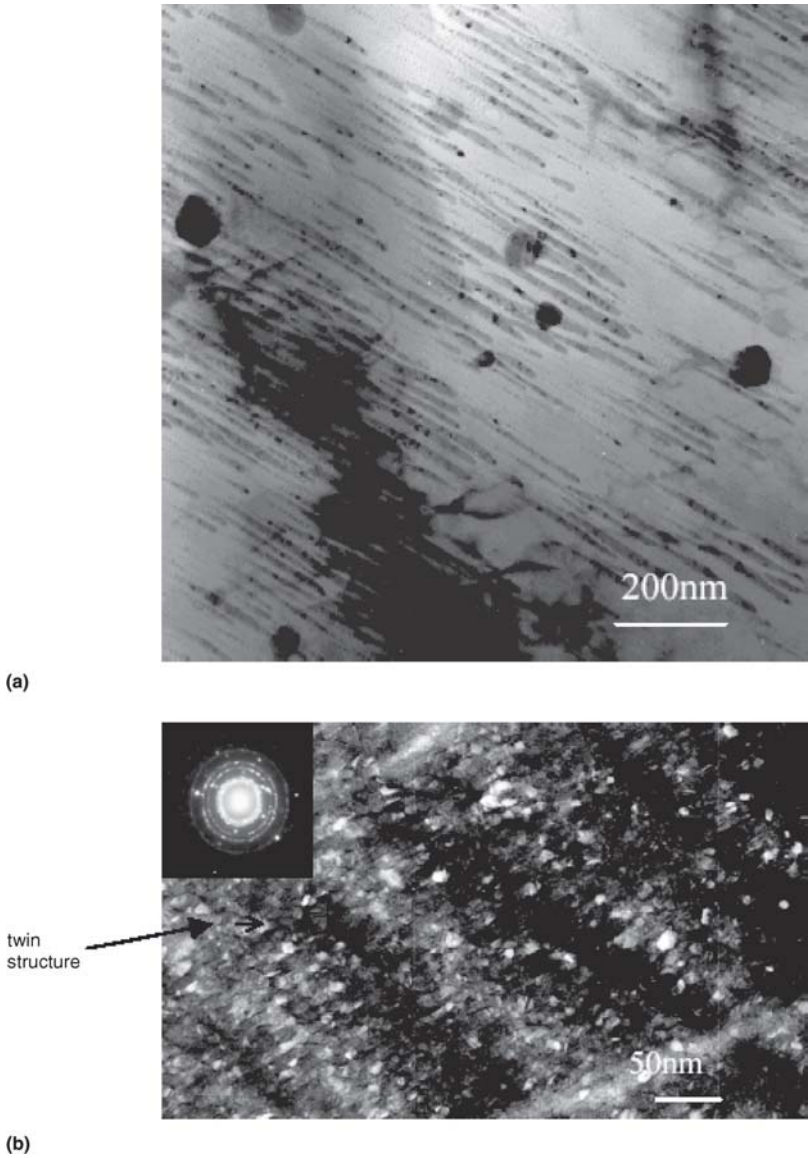

Fig. 5 (a) Mixed nanocrystalline structure and microbands at outer surface layer of the sample after the EUIT-1 process; the microband was well elongated along the rolling direction. (b) Microbands in the surface region (~7 μm) in the dimension about 10-15 nm wide and well elongated along certain direction; the twin structure was observed within the microbands.

corresponding decrease in the strain energy. TEM observations suggested that subgrains and microbands can also be formed. The subgrains have been measured at sizes between 8 and 10 nm at the top surface region and microbands in the order of 10-15 nm at the subsurface, which is comparable to that attained by USSP (Ref 19) and other SPD (Ref 14). Such a surface layer of ultrafine grain size explains the feature, originally named, "white layer structure," which was reported in a previous work (Ref 30). The grain structure of the 2024-T3 aluminum alloy after the EUIT process can be classified into the following: equiaxed ultrafine, nanograin (8-10 nm) structure at the top surface; equiaxed ultrafine grain structure mixed with extended microbands (10-15 nm) at a depth of approximately 3-5 μm; and refined grain on a nanoscale at less than 10 μm.

The EUIT process is accompanied by: ultrasonic impacts, which induce ultrasonic plastic deformation at the surface material; the distribution of ultrasonic stress waves that penetrate the subsurface material; and quick heating and cooling at the area of plastic deformations. The generated high strain rates result in the development of areas of high dislocation density and twining structure. It was observed the nanocrystalline region contained much higher dislocation density than the regular bulk grains (Fig. 9) and a twining structure appeared within the nanograin region (Fig. 4). The high dislocation density could be responsible for the production of new grain boundaries. Such subdivision may take place on a finer scale with the formation of microbands, and further straining of the newly formed subgrain could result into nanocrystallization. In addition, the pin vibration during the ultrasonic impact, with the surface material synchronously or in-phase and at the carrier frequency of the transducer, could change the slip path. Therefore, the dislocations not only interact with other dislocations in the current active slip systems but also interact with inactive dislocation generated from previous impacts. Such interaction will promote the formation of subgrains and further enhances the effectiveness of the grain refinement.

As mentioned above, the EUIT process is also accompanied

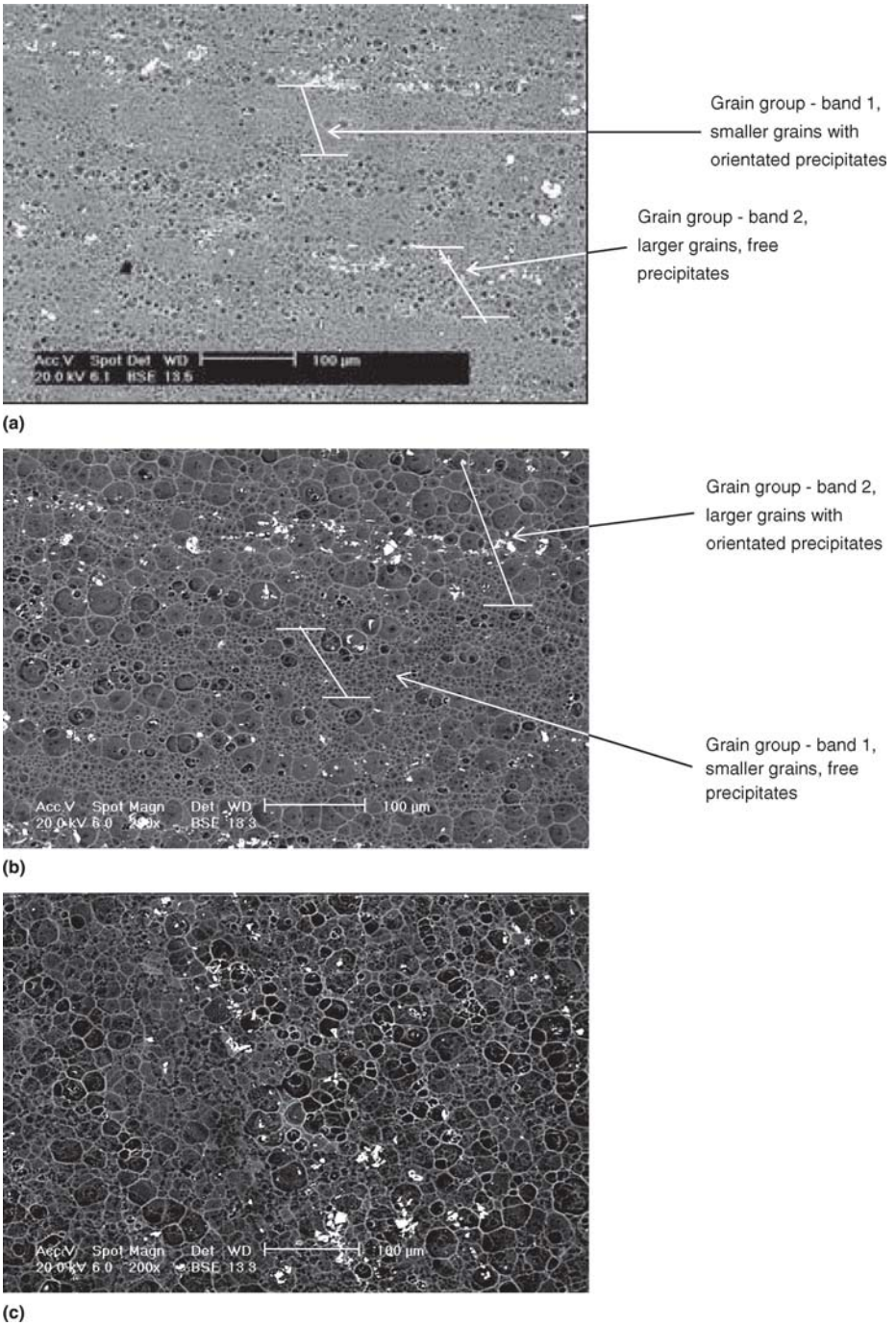

Fig. 6 Comparison of the grain size distributed in the samples shows grain size of different grain groups within the UIT samples (image was taken in sputtered etch sample at 2.6 μm depth from top surface): (a) EUIT1; (b) EUIT2; (c) bare

by rapid local heating of the material at the ultrasonic impact point and quick heat discharge from the same region. Therefore, it could be suggested that during the EUIT process, a geometric dynamic recrystallization may occur (Ref 31) in which larger strains with high angle boundaries are pushed together and are separated by subgrains. Further, the separation of the high angle boundaries is equal to the subgrain size; the rotation of the subgrain may occur gradually until all the dislocations are absorbed by the grain boundaries. The high angle boundaries impinge and a microstructure of small and equiaxed grains are formed (Fig. 3).

It was also observed that high density dislocation can be found in one grain and might disappear at the boundary, which suggests that the ultrasonic plastic strain induced grain boundary migration. Thus, the migrated boundary is free from dislocation structure. The driving force for strain induced grain boundary migration is presumed to arise from a difference in dislocation density on opposite sides of the grain boundary (Ref 32). Observation of the twin boundaries in this work further suggested that EUIT process provided a higher energy environment for the migrated boundary.

It is most interesting to note that EUIT caused the precipitates to migrate and separate into bands. Comparison with the "as-rolled/bare" state reveals that the size of the precipitates

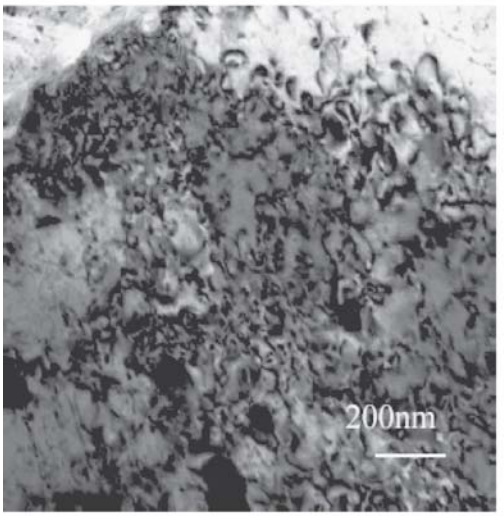

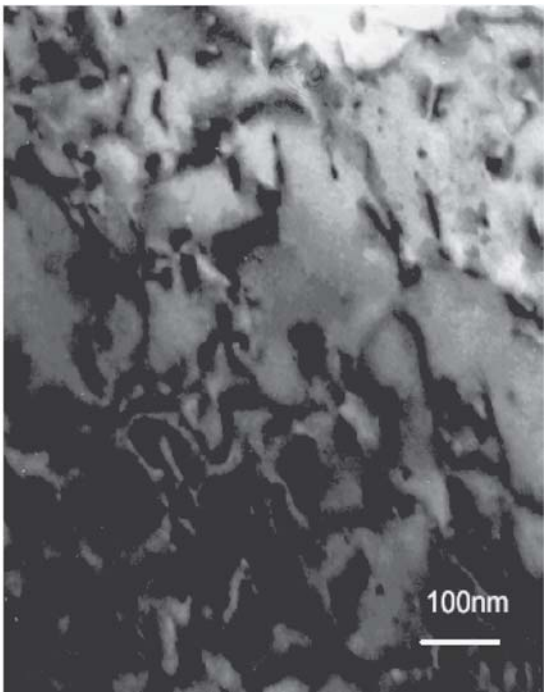

Fig. 7 High density dislocation cell at the surface region

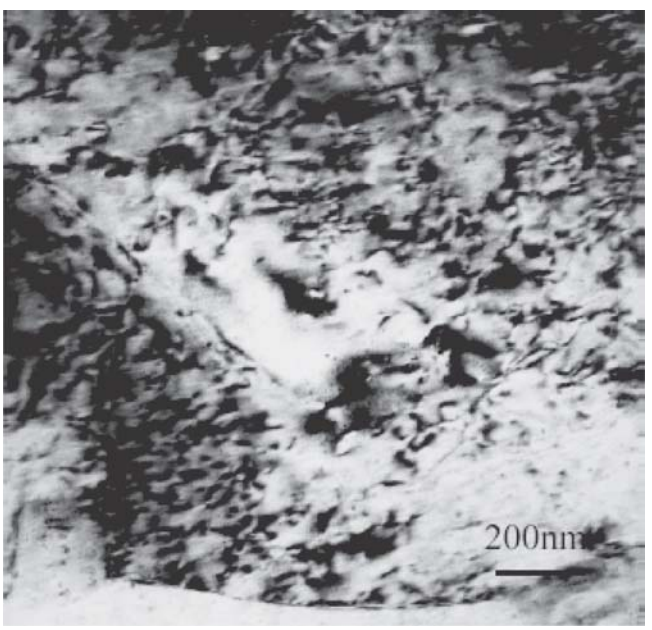

Fig. 8 High density dislocation at top surface region accompanied with nanocrystalline structure. The area is the same as that in Fig. 2, but the sample was titled at 10°.

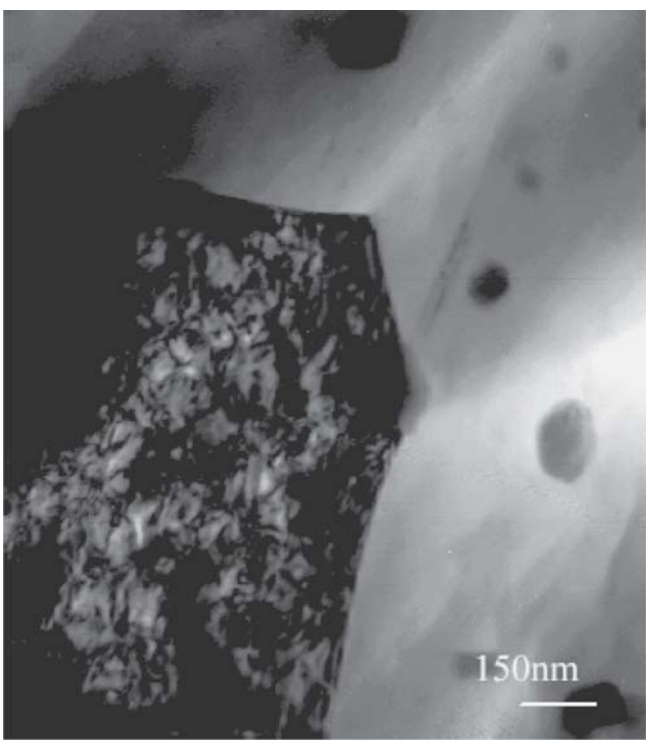

Fig. 9 TEM bright image shows the grain boundary as source of dislocation, which indicates the high-density dislocation tangle zone (DTZ) and the DTZ transformed into dislocation cells. The high density dislocation disappeared at the boundary.

after the EUIT exhibits a reduced scale, and their density shows maxima within the band. The reason behind such a phenomenon is not well understood; yet, speculative thinking suggests that this could be the result of the geometric dynamic recrystallization process in which the high energy and high temperature may achieve a critical energy and hence cause the precipices to facilitate a dissolution-coarsening mechanism.

TEM observations suggest that the subgrain size gradually increases from nanostructure (8-10 nm) at the top surface down to 10-15 nm at a subsurface region, which indicates that the grain size can change within the impact effect zone from the top surface down to the matrix due to strain variations. Such findings acknowledge the fact that the EUIT process parameters, such as impact frequency, amplitude under load, and feed

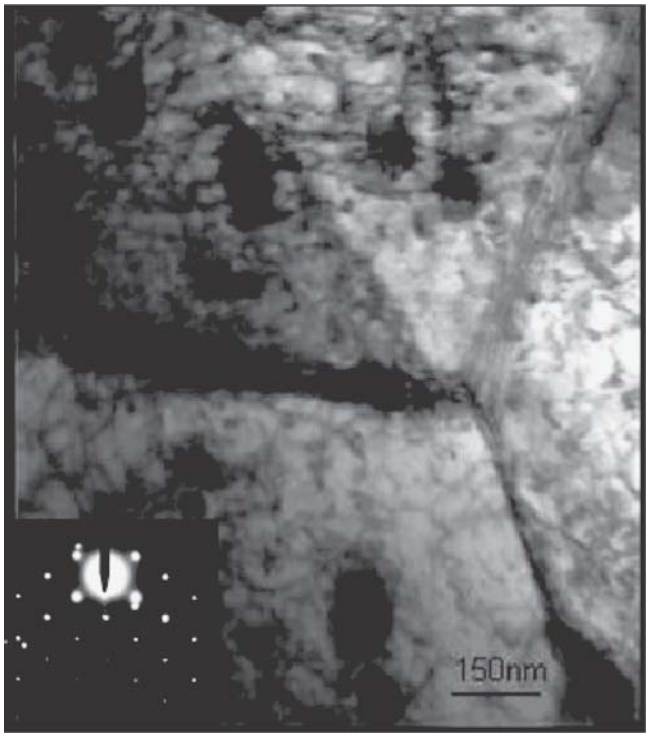

Fig. 10 Twin boundaries accompanied by high density dislocations within grain at deep surface layer of the alloy. The inset SAD was taken from the boundary area.

rate can control the average grain size and microstructure of the aluminum alloy. Figure 2 demonstrates that the feed rate mostly controls the surface effects and the amplitude under load is responsible for the penetration depth. For example, the most severe plastic deformation caused by the EUIT1 achieved a finer average grain size compared at a depth of 2.6 μm with EUIT2. Yet, the higher feed rate (EUIT2) achieved finer grain size at the surface, indicating the effect of the heating rate.

5. Conclusions

The surface layer microstructure of 2024-T351 Al alloy induced by the EUIT consists of nanocrystalline structure at the top surface with an average grain size of about 8-10 nm and elongated microbands about 10-15 nm wide at the near surface region. The affected zone was found to be approximately 10 μm accompanied by high density dislocations and twining structures.

The grain refinement process has been suggested to follow formation of high dislocation density and twining structure following further straining, formation of microbands structure, subdivision of microbands structure into submicron grains, and further breakdown of the subgrains to be equiaxed.

This work demonstrated that the EUIT process can effectively achieve nanocrystallization of the surface layer for the metal, which may lead to improvements in the corrosion and fatigue properties of the materials.

Acknowledgments

The authors would like to thank Applied Ultrasonics, USA and Airbus, UK for supporting this research work.

References

1. T. Hanlon, Y.N. Kwon, and S. Suresh, Grain Size Effects on the Fatigue Response of Nanocrystalline Metals, *Scripta Mater.,* 2003, **49,** p 675-680
2. F.J. Humphreys, B.P. Philip, and R. Priestner, Fine-Grained Alloys by Thermomechanical Processing, *Solid State Mater. Sci,* 2001, **5,** p 15-21
3. M. Niikura, M. Fujioka, Y. Adachi, A. Matsukura, T. Yokota, Y. Shirota, and Y. Hagiwara, New Concepts for Ultra Refinement of Grain Size in Super Metal Project, *J. Mater. Proc. Technol.,* 2001, **117,** p 341-346
4. Y. Satio, H. Utsunomiya, N. Tsuji, and T. Sakai, Novel Ultra-High Straining Process for Bulk Materials—Development of the Accumulative Roll-bonding (ARB) Process, *Acta Mater,* 1999, **47**(2), p 576-583
5. Z. Horita, D.J. Smith, M. Furukawa, M. Nemoto, R.Z. Valiev, and T.G. Langdon, Characterization of Ultrafine Grained Materials Produced by Torsion Straining, *Proc. Thermec '97 TMS*, T. Chandra and T. Sakai, Ed., 1997, TMS, p 1937-1943
6. A.K. Ghosh and W. Huang, Investigations and Applications of Severe Plastic Deformation Series, *High Technology*, Series 3, T.C. Lowe and Z. Valiev, Ed., Kuwer Acdemic, Boston, MA, 2000, p 80:29
7. J.Y. Huang, Y.T. Zhu, H. Jiang, and T.C. Lowe, Microstructures and Dislocation Configurations in Nanostructured Cu Processed by Repetitive Corrugation and Straightening, *Acta Mater.,* 2001, **49**(9), p 1497-1505
8. Y.T. Zhu and T.C. Lowe, Observations and Issues on Mechanisms of Grain Refinement during ECAP Process, *Mater. Sci. Eng.,* 2000, **A291,** p 46-53
9. J.W. Park, J.W. Kim, and Y.H. Chung, Grain Refinement of Steel Plate by Continuous Equal-channel Angular Process, *Scripta Mater.,* 2004, **51,** p 181-184
10. M.V. Markushev, C.C. Bampton, M.Yu. Murashkin, and D.A. Hardwick, Structure and Properties of Ultrafine Grained Aluminum Alloys Produced by Severe Plastic Deformation, *Mater. Sci. Eng.,* 1997, **A234-236,** p 927-931
11. F.J. Humphreys and M. Hatherly, *Recrystallization and Related Annealing Phenomena,* Pergamon Press, Oxford, UK, 1995
12. J.A. Wert, N.E. Paton, C.H. Hamilton, and M.W. Mahoney, Grain Refinement in 7075 Aluminum by Thermo-Mechanical Processing, *Metall. Trans.,* 1981, **12A,** p 1267-1276
13. R.Z. Valiev, R.K. Islamgaliev, and I.V. Alexandarov, Bulk Nanostructured Materials from Severe Plastic Deformation, *Prog. Mater. Sci.,* 2000, **45,** p 103-189
14. P.B. Prangnell, J.R. Bowen, and P.J. Apps, Ultrafine Grain Structures in Aluminum Alloys by Severe Deformation Process, *Mater. Sci. Eng.,* 2004,**A375-377,** p 178-185
15. R.Z. Valiev, Structure and Mechanical Properties of Ultrafine-Grained Metals, *Mater. Sci. Eng.,* 1997, **A234-236,** p 59-66
16. E. S. Statnikov, Guide for Application of Ultrasonic Impact Treatment for Improving Fatigue Life of Welded Structures, IIW, Doc. XIII-1757-99, International Institute of Welding, 1999
17. N.R. Tao, M.L. Sui, J. Lu, and K. Lu, Surface Nanocrystalline of Iron Induced by Ultrasonic Shot Peening, *NanoStruct. Mater,* 1999, **11**(4), p 433-440
18. G. Lu, J. Lu, and K. Lu, Surface Nanocrystalline of 316L Stainless Steel Induced by Ultrasonic Shot Peening, *Mater. Sci. Eng.,* 2000, **A286,** p 91-95
19. X. Wu, N. Tao, Y. Hong, B. Xu, J. Lu, and K. Lu, Microstructure and Evolution of Mechanically-Induced Ultrafine Grain in Surface Layer of Al-alloy Subjected to USSP, *Acta Mater.,* 2002, **50,** p 2075-2084
20. K.Y. Zhu, A. Vassel, F. Brisset, K. Lu, and J. Lu, Nanostructure Formation Mechanism of α-Titanium Using SMAT, *Acta Mater,* 2004, **52,** p 4101-4110
21. E.Sh. Statnikov, V.N. Vityazev, and O.V. Korolkov, Study of Comparative Characteristics of Ultrasonic Impact and Optimization of Deformation Treatment Processes, *5th World Congress on Ultrasonics,* Paris, France, 2003
22. I.I. Mukhanov and Yu.M. Golubev, Strengthening Steel Components by Ultrasonically Vibrating Ball, *Vestn. Mashin*, 1966, **11,** p 52-53, in Russian
23. E.S. Statnikov, "Development and Study of Ultrasonic Specific-Purpose Devices," Thesis, Academician N.N. Andreyev Acoustic Institute, Academy of Sciences of the USSR, 1982
24. E.S. Statnikov and V.F. Kazantsev, Ultrasonic Surface Plastic Defor-

mation of Solids, *Effect of High-intensity Ultrasound on Interphase Metal Surface,* A.I. Manokhin, Ed., Academy of Sciences of USSR, Moscow, Nauka, 1986, Chap. 5, p. 186-216
25. V.M. Lihavainen, G. Marquis, E.S. Statnikov, Fatigue Strength of a Longitudinal Attachment Improved by Ultrasonic Impact Treatment, IIW Doc. IIW-1631-03, *Welding in the World,* 2004, **48**(516), p 67-75
26. E. S. Statnikov, V.O.Muktepavel, V.N.Vityazev, V.I.Trufyakov, V.S.Kovalchuk and P.Haagensen, Comparison of the Improvement in Corrosion Fatigue Strength of Weld Repaired Marine Cu 3-grade Bronze Propellers by Ultrasonic Impact Treatment (UIT) or Heat Treatment, IIW Doc. XIII-1964-03, International Institute of Welding, 2003
27. J. Janosch, H. Koneczny, S. Debiez, E.Sh. Statnikov, V.I. Trufyakov, P.P. Mikheev, Improvement of Fatigue Strength in Welded Joint (in HSS and Aluminum Alloy) by Ultrasonic Hammer Peening, IIW-1300-95, *Welding in the World,* 1996, **37**(2), p 72-83
28. S. Roy, J.W. Fisher, B.T. Yen, Fatigue Resistance of Welded Details Enhanced by Ultrasonic Impact Treatment (UIT), *Int. J. Fatigue,* 2003, **25**(9-11), p1 239-1247
29. Haagensen, P.J., E.S. Statnikov, L. Lopez-Martinez, Introductory Fatigue Tests on Welded Joints in High Strength Steel and Aluminum Improved by Various Methods Including Ultrasonic Impact Treatment (UIT), IIW, Doc. XIII-1748-98, International Institute of Welding, 1998
30. E.S. Statnikov, Ultrasonic Impact Methods for Treatment of Welded Structure, US Patent 6 338 765, 2002.
31. H.J. McQueen, O. Knustad, N. Ryum, and J.K. Solberg, Microstructure Evolution in Al Deformed to Strains of 60 at 400 °C, *Scripta Mater.,* 1985, **19,** p 73-78
32. F.J. Humphreys and M. Hatherly, *Recrystallization and Related Annealing Phenomena,* Pergamon, 1995, Chap. 6